Journal of the Optical Society of Korea
Vol. 13, No. 3, September 2009, pp. 341-348

DOI: 10.3807/JOSK.2009.13.3.341

Scientific and Engineering Applications of Full-field Swept-source Optical Coherence Tomography

Dalip Singh Mehta*, Tulsi Anna, and Chandra Shakher

Laser Applications and Holography Laboratory, Instrument Design Development Centre, Indian Institute of Technology Delhi, Hauz Khas, New Delhi 110016, India

(Received June 3, 2009 : revised August 29, 2009 : accepted August 31, 2009)

We report the development of full-field swept-source optical coherence tomography (SS-OCT) in the wavelength range of 815-870 nm using a unique combination of super-luminescent diode (SLD) as broad-band light source and acousto-optic tunable filter (AOTF) as a frequency-scanning device. Some new applications of full-field SS-OCT in forensic sciences and engineering materials have been demonstrated. Results of simultaneous topography and tomography of latent fingerprints, silicon microelectronic circuits and composite materials are presented. The main advantages of the present system are completely non-mechanical scanning, wide-field, compact and low-cost.

Keywords: Optical coherence tomography, Instrumentation, Microscopy, Phase measurement and nondestructive testing

OCIS codes: (170.4500) Optical coherence tomography; (170.0180) Microscopy; (120.0120) Instrumentation, measurement, and metrology; (120.5050) Phase measurement; (120.4290) Nondestructive testing

I. INTRODUCTION

Optical coherence tomography (OCT) is a non-contact, non-destructive, cross-sectional imaging modality based on the principle of low-coherence interferometry [1,2]. The first OCT was realized in 1991 by Huang et. al. [1,2] and they demonstrated the non-invasive, cross-sectional imaging of biological samples. Since then OCT has become one of the most important techniques for biomedical imaging and diagnostics due to its ultrahigh resolution and high sensitivity. Broadly, OCT can be divided into two categories: time-domain OCT (TD-OCT) and Fourier-domain OCT (FD-OCT) [2-8]. The FD-OCT is further divided into two categories one is spectral-domain OCT (SD-OCT) and the other one is swept-source OCT (SS-OCT). FD-OCT has many advantages over TD-OCT, i.e., it has high signal-to-noise ratio, high imaging speed and the interference signal is detected as a function of wavelength and hence the depth information is retrieved without mechanically scanning the reference mirror as is done in TD-OCT [1, 2]. FD-OCT that uses a broadband light source and a spectrometer at the detector arm, is called spectral-domain OCT (SD-OCT) [2-7]. Another version of FD-OCT is called swept-source OCT (SS-OCT) in which a fast tunable laser system is used at the input of the OCT [8,9]. In this technique wavenumber is time encoded over a large optical bandwidth by rapidly tuning a narrow-band source. Since the amplitude and phase of the detected signal at each wavelength is directly related with spatial modulation of the refractive index distribution, axial or depth scattering profile is obtained by analyzing the sample reflectivity as a function of wavelength.

Recently there has been great progress in the development of fast tunable laser systems which have been used for OCT, optical metrology and biomedical imaging. Several wavelength-tuning laser systems and filters, such as inter-cavity spectral filters consisting of a diffraction grating and polygon mirror [10], superluminescent diode (SLD) and a tunable fiber Fabry-Perot (FFP) filter [11], external cavity semiconductor laser using a reflection grating, a focusing lens and mirror/slit assembly [12], a Ti:sapphire laser system driven by a cw stepper-motor [13] and a specially designed acousto-optic tunable element [14] have been developed and used in SS-OCT. But all these swept-source combinations, in spite of having many advantages, use mechanical scanning to

*Corresponding author: dsmehta@iddc.iitd.ac.in

tune the wavelength. Further, in all these systems the optical set-ups are complicated, bulky and expensive. We have developed a SS-OCT in the wavelength range of 815-870 nm using a unique combination of SLD as broad-band light source and acousto-optic tunable filter (AOTF) as a frequency-scanning device [15–17]. The main advantages of the present tunable system are broad range of tunability, non-mechanical scanning because AOTF is an electronically controllable device. Further, the conventional OCT interferometer system was modified by coating aluminum oxide on one side of the beam-splitter which is used as reference mirror, thus making the OCT system more compact, nearly common-path and totally non-mechanical scanning.

The current applications of OCT range from biomedical imaging and diagnosis [2-4] to the characterization of polymer microstructures of paper [18] and paint industry [2] to the reading of multi-layered storage media [2-4]. In the area of biology it has been a cutting edge technology for biomedical imaging, diagnosis, ophthalmology, dentistry, dermatology, endoscopy, surgical guidance and cancer detection [1-6]. Although having been used in biomedical imaging and other disciplines for a decade, the technique has still not been able to catch the attention of researchers in the area of forensic sciences, semiconductor devices, Silicon integrated circuits (ICs) and composite materials. We demonstrate applications of full-field SS-OCT system, i.e., for the detection of latent fingerprints and simultaneous topography and tomography of engineering materials, such as, silicon microelectronic circuits and composite materials. Details of experimental set-up and results are presented.

II. PRINCIPLE OF FULL-FIELD SS-OCT

In full-field SS-OCT two-dimensional spectral interferograms are recorded as a function of varying wavelength of the swept-source. The spectral interferograms are recorded by an area detector and stored in the computer for further processing. The depth information z, from different layers of the sample can be retrieved simultaneously from the frequency of interference fringes without any reference arm modulation. If $S(k)$ is the spectral density of the source, R_R and R_S are reflectivities of reference and sample arms respectively then detected spectral intensity at interferometer output is given by [15]

$$I(x,y;k)=S(k)R_R+S(k)\int_{-\infty}^{\infty}\int_{-\infty}^{\infty}\sqrt{R_S(x,y,z)R_S(x,y,z')}e^{j[k|(z-z')+\phi(z)-\phi(z')]}dzdz' +2S(k)\sqrt{R_R}\int_{-\infty}^{\infty}R_S(x,y,z)\cos[kz+\phi(z)]dz \quad (1)$$

where z is optical path difference between sample and reference arms and ϕ is the phase shift. The first two terms in Eq. (1) are the DC components, one represents reflected intensity from reference mirror and the second term gives the mutual interference of the reflected signals from different surfaces within the sample, respectively. Depth information z, of the sample is retrieved from the last term by taking the inverse Fourier transform from k-domain to z-domain. In SS-OCT where wavelength is tuned in a regular manner across the source spectrum, wave number k is a function of time i.e., k=k (t).

$$\text{If} \quad P(x,y;k)=2S(k)\sqrt{R_R}\int_{-\infty}^{\infty}R_S(x,y,z)\cos[kz+\phi(z)]dz \quad (2)$$

$$\text{then,} \quad FFT^{-1}[P(x,y;k)]=f(x,y;t-\tau)+f(x,y;-t-\tau) \quad (3)$$

Here, $f(x,y,t)$ is the correlation product between reference and sample fields. The two terms in Eq. (3) are mutual mirror images as Fourier transform of a real function is Hermitian. Time delay corresponds directly to distance z. For complex samples, a multiple-peak Fourier spectrum is obtained. By selective filtering of peaks, complete depth information i.e.; amplitude and phase both of the desired surface can be determined.

III. EXPERIMENTAL DETAILS

A non-mechanical scanning full-field SS-OCT system includes a swept-source system using broad-band low coherence (SLD) as light source and an AOTF as tunable filter [15-17]. The AOTFs are solid-state electronically tunable optical filters that select precise wavelengths by applying an appropriate RF-frequency and hence no mechanically moving parts are required. RF-frequency applied to an AOTF transducer controls the transmitted (filtered in 1st order) wavelength. Thus it provides a fine-tuned nearly monochromatic light. Further, AOTFs have high-speed of operation of the order of a few microseconds, large range of tunability (600-1200 nm) and linear wavenumber-RF-frequency characteristics. Thus, changing the wavelength of broad-band light using AOTF is easier and less expensive. One promising development in AOTFs is that they are already commercially available. Light emitted by SLD was coupled to the input of AOTF through a polarization maintaining single mode optical fiber connected through an FC connector to avoid back reflections into SLD [15-17]. The beam was collimated using a convex lens. Area of illumination on the sample was sufficiently large (5 mm×5 mm) that it eliminates the need of lateral scanning (B-scan). Both the SLD and AOTF were characterized using a high-resolution spectrometer (HR 4000 Ocean Optics Ltd.). Figure 1 (a) shows the spectral distribution of SLD. It has two spectral centers at 819.55 nm and

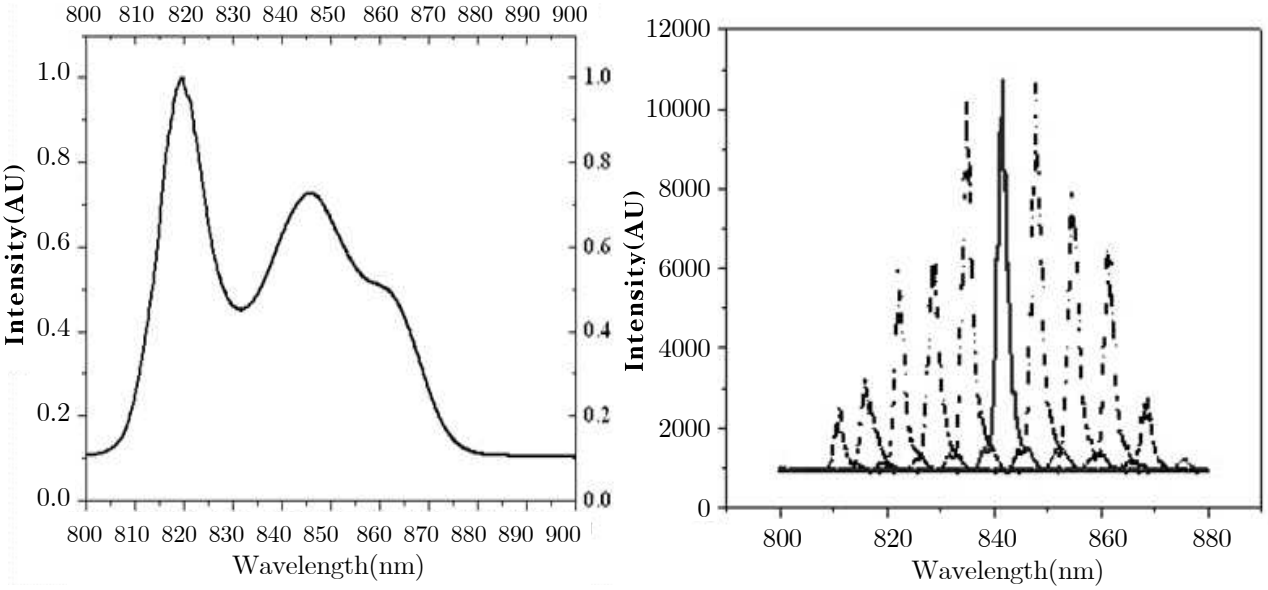

(a) (b)

FIG. 1 (a) Spectrum of SLD, (b) Tuned spectra at the output of AOTF at different RF-frequency.

845.82 nm with spectral bandwidth (FWHM) of 48.38 nm. At the input current of 174 mA (temperature 25℃), the peak power of SLD is 7.5 mW. On applying RF-frequency to acousto-optic crystal (TeO_2) electronically, output of AOTF was measured both at constant frequency as well as by sweeping the frequency. The light transmitted by AOTF is quasi-monochromatic (QM) and spatially coherent. Figure 1 (b) shows the tuned spectra at the output of AOTF recorded by high-resolution spectrometer with varying RF-frequency. Spectral bandwidth (FWHM) of the frequency-tuned light is~1.5 nm over entire wavelength scan range of SLD, i.e., 800-870 nm. The RF-frequency was changed linearly with a constant step of 0.2 MHz and tuned spectrum was recorded using a spectrometer. A linear relationship between RF-frequency and peak wavelength was obtained. Thus by scanning the wavelength of broad-band light from SLD using AOTF, a frequency-tunable quasi-monochromatic swept-source was realized. Assuming the SLD spectrum and AOTF tuned spectrum nearly Gaussian [2], we calculated the coherence length l_c

$$l_c = \frac{4\ln 2}{\pi}\frac{\lambda_0^2}{\Delta\lambda} \tag{4}$$

The axial (also known as vertical) resolution of conventional OCT systems that use low numerical aperture (N.A.) objective lenses is determined by the coherence length of the source alone and is found to be half of the coherence length [2]. The transverse resolution (Δx) also known as lateral resolution of the SS-OCT can be given by the following expression [2];

$$\Delta x = 1.22\frac{\lambda}{2[N.A.]} = 0.61\frac{\lambda}{N.A.} \tag{5}$$

For SLD, $\Delta\lambda$= 48.38 nm and average central wavelength λ_0=842.5 nm, l_c=12.954 μm giving axial resolution of about 6.48 μm. For a RF-frequency step of 0.2 MHz applied to AOTF, the corresponding change in the wavelength of AOTF spectrum i. e., line width was found to be 1.50 nm. With $\Delta\lambda$=1.5 nm and λ_0=842.5 nm, coherence length increases to 0.418 mm for the AOTF. Currently AOTF's are commercially available with spectral resolution of the order of 0.1 nm that leads to a large coherence length. This choice can be utilized in probing large depth of penetration of the sample.

IV. RESULTS AND DISCUSSION

1. Application of Full-Field SS-OCT In Forensic Sciences

The developed full-field SS-OCT was used for the reconstruction of latent finger prints [15,16]. Fingerprinting is one of the most widely used methods by forensic scientists for identifying and authenticating individuals [19, 20]. Depending upon their formation processes, there are two types of fingerprint data; exemplar fingerprints and latent fingerprints [19,20]. The former is acquired directly from human fingers using specific fluids or scanners in controlled environments. But usually, it is latent fingerprints that are left at crime scenes and require great effort to render them visible, as the surfaces on which they are left, possess varying physical and chemical compositions. When a finger comes into

contact with any surface, fingerprint impression gets imprinted on it due to the dielectric residue corresponding to the ridges of the fingerprint while the furrow area, being at depth leaves no impression as such. Therefore, amplitude of the reflected signal from impression due to ridges and furrows differs depending upon the property of residue and the surface bearing the impression. Two latent fingerprints were prepared for the study. The first sample was a fingerprint impression taken on a glass substrate using a white fluid. Second sample was an impression of a fingerprint sandwiched between a glass substrate and a cover slip. Placing a cover slip over the fingerprint impression reduces its reflectivity. The second sample was placed in the interferometric arm and was imaged using a camera zoom lens that was placed at 10 cm from the Beam splitter (BS) facing the reference arm. RF-frequency to AOTF was tuned sequentially with a constant step of 0.1 MHz. Total of 81 interferograms were recorded using a charged coupled device (CCD) detector (Roper Scientific, Inc.) having 1392×1024 pixels with each pixel size 6.5 μm×6.5 μm. Figure 2 (a) shows the example of an interferogram taken at 91 MHz (843.69 nm) and Fig. 2 (b) provides information about corresponding Fourier transform. It can be seen from Fig. 2 (a) that the interference fringes are multiplexed, due to multiple reflections from the cover slip, finger prints and glass substrate. Inverse FFT of the peak-1 gives brightness distribution of the cover slip i.e., top surface of the sample as shown in Fig. 2 (c). Fingerprint information is retrieved from selective filtering of the 2nd peak (Peak-2) as shown in Fig. 2 (d). Optical path length between the top surface

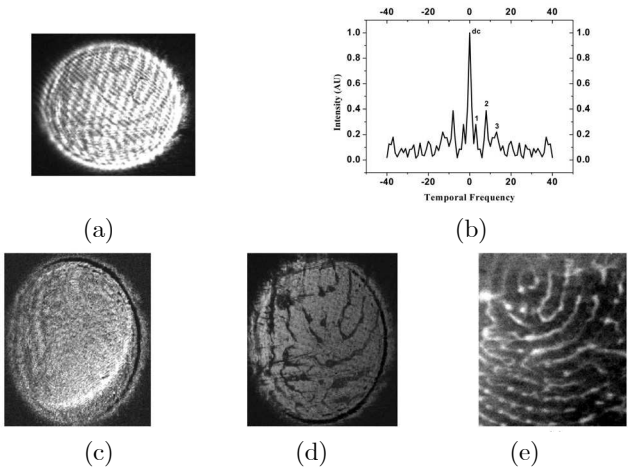

FIG. 2. (a) An example of interferogram at 91 MHz, (b) Fast Fourier transform of the time-varying interference fringe signal, (c) Reconstructed OCT image of the sample filtered at 1st order peak, (d) Reconstructed OCT image of the sample filtered at 2nd order peak, and (e) Image of the fingerprint impression taken with high-resolution camera *(Reprinted with permission from [15]. © 2007 American Institute of Physics).*

of the cover slip and the fingerprint was calculated from Fig. 2 (b) and found to be ~ 140 μm which is below the coherence length of the present system. Amplitude of peak-2 corresponding to fingerprint impression is higher compared to peaks 1 and 3 as shown in Fig. 2 (b). Figure 2 (e) is the image directly taken using digital camera under high brightness lighting conditions. Though the fingerprint impression was buried inside the cover slip, it was possible to reconstruct it using the present full-field SS-OCT system. We have also reconstructed phase maps of the latent fingerprints thus giving simultaneous topography and tomography of fingerprints from the same experiment [16]. The main advantage of the present system for fingerprint detection is that it uses the low coherence interferometry for reconstruction. Therefore, the present technique may find finer details of the object.

2. Application of Full-Field SS-OCT for Silicon-Microelectronic Circuits

Imaging and measurement of silicon integrated circuits (ICs) and thin-film multilayer structures are of great importance in the development of ongoing miniaturization of semiconductor devices. The precise measurements of film-thickness and sub-surface imaging of ICs nondestructively are important for industrial applications. Various optical methods have been developed and realized for imaging and functional defect-detection of micro-electromechanical system (MEMS) based silicon ICs [17]. We demonstrate simultaneous topography and tomography of micro-electro mechanical systems based on silicon ICs using full-field SS-OCT [17]. The optical set-up consists of a swept-source system, a compact Michelson interferometer and an area detector. By means of sweeping the frequency of the light source, multiple interferograms were recorded and both amplitude and phase map of the interference fringe signal were reconstructed. Optically sectioned images of the silicon ICs circuits were obtained by selective Fourier filtering and the topography was retrieved from the phase-map. The main advantages of the proposed system are completely non-mechanical scanning, easy for alignment, high-stability because of its nearly common-path geometry and compactness. Interferograms were recorded by CCD camera and analyzed using an algorithm written in MATLAB software. Figure 3 (a) shows the example of an interferogram recorded at RF of 91 MHz for the silicon IC. Interferograms for the entire tuned spectrum were stacked together along the wavelength axis and corresponding variation of intensity along the wavelength axis was computed at each pixel. Fast Fourier transform (FFT) of the interference fringe signal was then computed providing multiple peaks as shown in Fig. 3 (b) corresponding to different depth layers of the object. The first order peak in Fig. 3 (b) corresponds to the shortest depth position. Other higher order peaks correspond to different axial

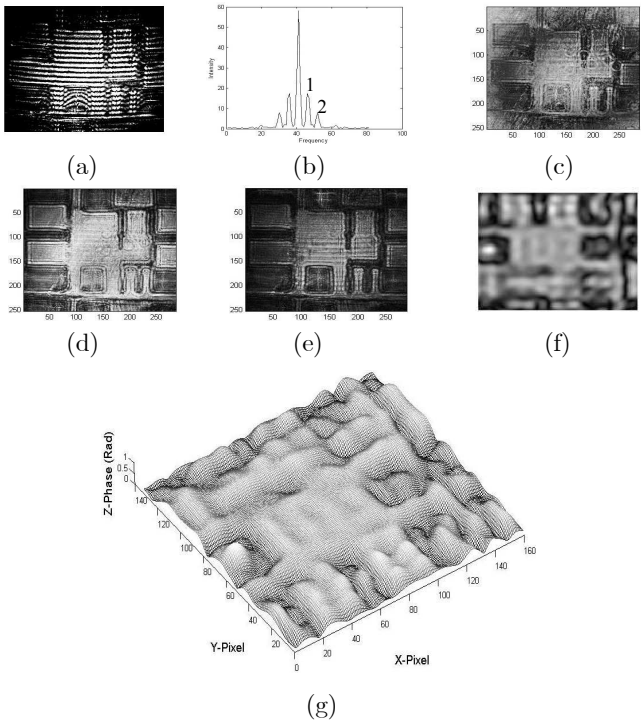

FIG. 3. (a) An example of interferogram at 91 MHz using silicon IC, (b) Fourier spectrum of the interference fringe signal for the stacked interferograms, (c)-(e) reconstructed OCT images and the corresponding reconstructed phase profiles (g) gray level image and (h) mesh structure of the IC sample related to image (d).

positions of the silicon IC. Optically sectioned images of the silicon IC were obtained by selective Fourier filtering of each peak and the corresponding topography was retrieved from the phase-map. Figures 3 (c) - (e) shows the reconstructed OCT images of the silicon IC at different depth positions. Figure 3 (c) belongs to a particular axial position and was obtained at selective Fourier filtering closer to the dc-component hence detailed features of the IC's are not revealed in this figure.

Best optically sectioned image was obtained by means of filtering the prominent first order peak (peak 1 as shown in Fig. 3 (b)) as can be seen from Fig. 3(d). It can be seen from Fig. 3 (d) that many details about IC are visible such as small aluminum square pads around the corner of the IC and other connecting conductors. We changed the filter position and by means of filtering peak 2 as shown in Fig. 3 (b) the optically sectioned image of the central part were resolved more clearly as shown in Fig. 3 (e). Fourier filtering at higher order means the larger depth range and hence one can also obtain sub-surface imaging. We also computed the phase map of the silicon IC corresponding to the best reconstructed amplitude image i.e., Fig. 3 (d). Figure 3 (f) is a gray level image which shows the reconstructed phase map. Figure 3 (g) shows the 3-D mesh pattern of the phase map shown in Fig. 3 (f). From this Fig. it can be seen that the phase variations of the central aluminum pad and the small square blocks along the side are clearly visible. The images are slightly blurred, this is because we used low numerical aperture lens and there may be slight defocusing of the object. Our study reveals that the current full-field SS-OCT may lead to volumetric and subsurface imaging of inorganic and organic semiconductor multilayer structures non-destructively with high resolution. The present system is totally non-mechanical scanning, and a wide and hence large area of sample can be imaged at a time.

3. Application of Full-Field SS-OCT for Structural Characterization of Composite Materials

Composite materials are obtained by holding together two or more elements by a matrix in a manner such that the properties of the resultant material are very different from the properties of its constituents [21,22]. The matrix can be physical or chemical material that binds together a cluster of fibers or fragments of a much stronger material called the reinforcement. Physical matrix includes anything from physical entanglement and non-woven technologies to porous containers whereas chemical matrices range from hydrogen bonding to covalent bonding using resins and adhesives [21,22]. In other words, composites employ the fundamental principle of a fibrous reinforcement improving the properties of the matrix in which that reinforcement is contained. This results in a homogeneous but unalloyed mixture of two completely dissimilar materials conferring their distinct properties to each other without the loss of separate identity or characteristics. The greatest advantage of composite materials is strength and stiffness combined with lightness and durability. Commonly used techniques for polymer composite characterization are wide angle X-ray diffraction (WAXD), small angle X-ray scattering (SAXS), scanning electron microscopy (SEM), transmission electron microscopy (TEM), scanning tunneling microscopy (STM) and atomic force microscopy (AFM) [21,22]. They provide images of the surface features at atomic level. Except SAXS which is used to observe the surface features of the order of 10 Å or larger all the techniques give sub nanometer or finer structural information. However, they are quite sophisticated and expensive and require a substantial amount of preprocessing such as staining the sample with chemicals and embedding them in epoxy.

We developed a high-resolution full-field SS-OCT based on Linik interference microscope in the characterization of composite materials as shown in Fig. 4. The full-field SS-OCT optical set-up includes a swept-source system, an interference microscope and an area detector as shown in Fig. 4. Light emitted by SLD was coupled to the input of AOTF through a polarization maintaining single mode optical fiber connected through an FC connector to avoid back reflections into SLD. Interference microscope is based on a Linik interferometer

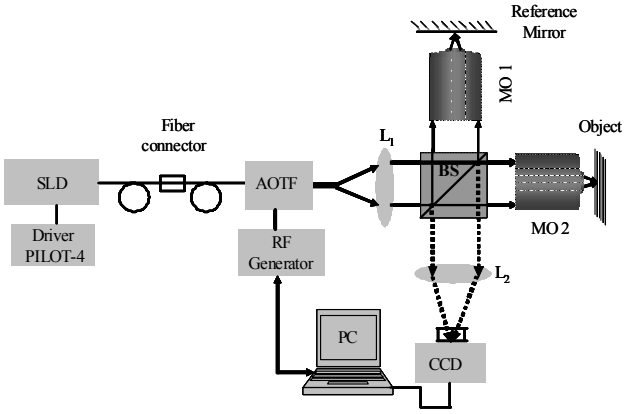

FIG. 4. Schematic diagram of full-field swept-source optical coherence tomographic system based on Linik interference microscope.

i.e., a Michelson interferometer with microscope objectives with 10 X magnification each in both arms focused inside the sample and onto a plane reference mirror. In contrast to the OCT systems based on Michelson and Mirau geometries, optical path lengths and focusing in each arm can be adjusted independently in this configuration. Use of two high numerical aperture (NA) objectives improves the spatial resolution similar to that of confocal microscopy. Full-field illumination and the parallel detection scheme adopted in the present study gives it an edge over conventional OCT systems. Axial resolution of conventional OCT systems that use low NA objectives is determined by the coherence length of the source alone and is found to be half of the coherence length [4]. Axial resolution of the tomographic images obtained using the Linik type interference microscope depends upon both the coherence length and the NA of objectives. Without time modulation, intensity of the detected flux at CCD is a function of distance z between the object and the focus plane and can be expressed as [23,24]

$$I(z) = \bar{I} + AF_{S,NA}(z) \tag{6}$$

where $\bar{I}$ is the average intensity and A is the amplitude of the interference signal. It can be seen from Eq. 6, $F_{S,NA}$ is the function of both coherence length of the source and the NA as opposed to the conventional OCT systems where it is the function of coherence length only. The function can be further expressed as [23,24]

$$F_{S,NA}(z) = \frac{1}{\sin^2\theta_{\max}} \int_0^{\infty} S(k) \int_0^{\theta_{\max}} \cos(2kz\cos\theta)\sin 2\theta d\theta dk \tag{7}$$

where $NA = n\sin\theta_{\max}$ with n being the refractive index of the medium. Contribution of high NA objectives alone to the axial resolution of the OCT image is given by [23,24]

$$\Delta z = \frac{0.44\lambda}{n(1-\cos\theta_{\max})} \tag{8}$$

Therefore, OCT images with ultra-high axial resolution can be obtained by properly selecting the source and the objective lenses. Lateral resolution which is a function of NA, automatically improves with the use of high NA objective in the present configuration. Like the axial resolution, lateral resolution also deteriorates to some extent inside the turbid medium due to reduction in effective NA and also due to multiply scattered signal.

The full-field SS-OCT system was applied for structural characterization and diagnosis of composite materials. Surface geometries of the matrix and reinforcement material can be characterized owing to the virtue of their varying scattering properties. Contents of different constituents can also be determined by analyzing the refractive index variation of the material. We had chosen different samples for this study. One of the samples was a composite of ultra high molecular weight (UHMW) polyethylene and resin which is used in the fabrication of bulletproof jackets. Figure 5 (a) shows the photograph of the composite material under study. Structural details are not visible from this Fig. An interferogram of the sample at 830 nm, intensity profile for the complete data cube at a particular pixel position and corresponding FFT are shown in Figs. 5 (b) & (c). Figure 5 (d) shows the Fourier spectrum of the interference fringe signal. OCT depth scans of UHMW polyethylene composite sample along the axial direction are shown in Figs. 5 (e)-(h). Different constituents at varying depth positions are easily reconstructed using the present technique. OCT depth scans of two layers which are similar in nature are shown in Figs. 5 (e) and (h). These two layers are combined using resin which can be seen in Fig. 5 (f). Figure 5 (g) shows the local variation of one of the layers at a particular axial position. Local variations at a particular depth can be estimated with the phase maps of the OCT scans. This can be utilized in extracting the information not only regarding the spatial position of the glass fiber but in getting an overview of other properties as well such as absorption and roughness etc. From this study we conclude that the composite materials being multilayer structure of different materials are highly scattering and are difficult to analyze by conventional imaging tools. Under these circumstances full-field SS-OCT is a potential candidate for the structural studies of composite materials. The main advantages of the present system are non-mechanical scanning and high-resolution and one can obtain simultaneous topography and tomography of the composite material. In the present system the SLD with 7.5 mW and AOTF were used to construct the swept-source. The optical power after passing through the AOTF is

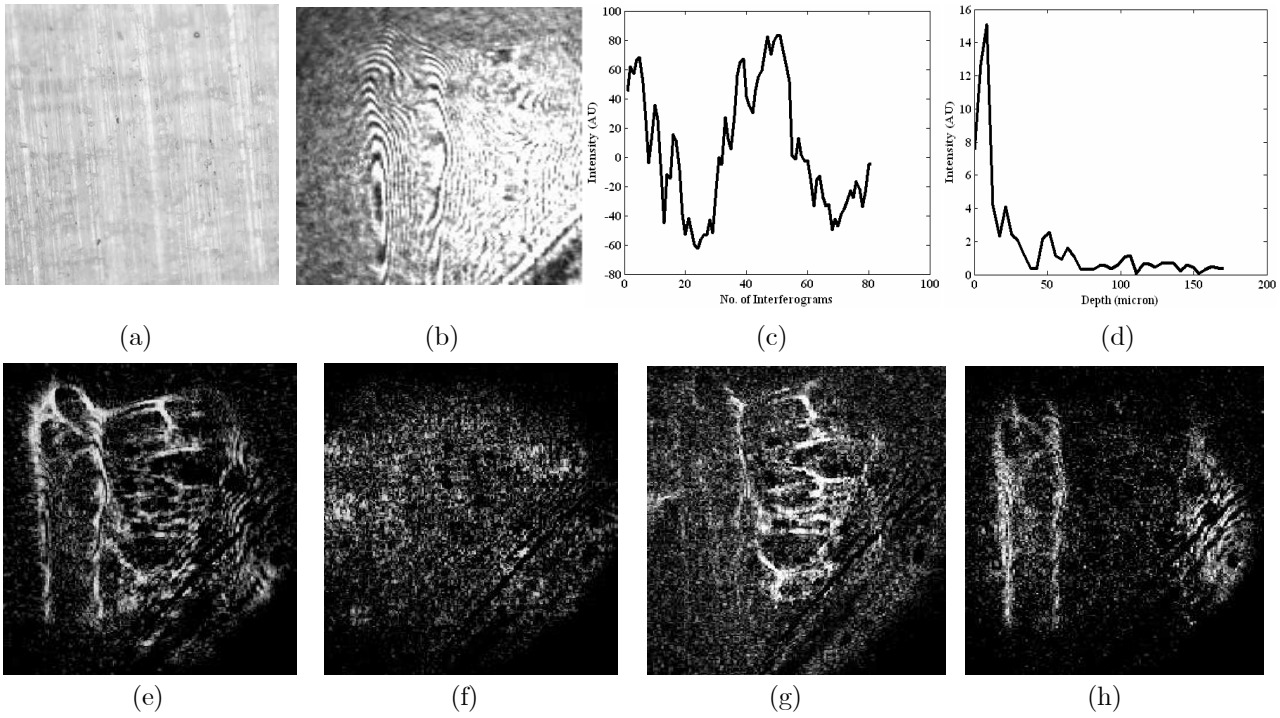

FIG. 5. (a) Photograph of the composite material, (b) An interferogram at 830 nm, (c) Interference fringe signal, (d) Fourier spectrum, and (e)-(h) are the optically sectioned OCT images of composite material at different axial positions.

of the order few hundred microwatts per tuned wavelength, which is relatively low power for highly scattering and low reflecting objects. The AOTFs are electronically controlled device and their response time is of the order of ~10 microseconds. But in the present OCT system the use of a low frame rate CCD camera (10 frames per second) limits the response time. The existing system can be further improved by using a high-speed CMOS/CCD camera with smaller pixel size and having the same speed as the AOTF of the order of ~ microseconds.

V. CONCLUSION

We have developed a full-field swept-source optical coherence tomographic (SS-OCT) system in the wavelength range of 815-870 nm using an unique combination of SLD as broad-band light source and acousto-optic tunable filter (AOTF) as a frequency-scanning device. The main advantages of the developed system are completely non-mechanical scanning, easy for alignment, high-stability because of it's nearly common-path geometry and compactness. Some new applications of full-field SS-OCT have been described and demonstrated. The full-field SS-OCT was first applied for the detection of latent finger prints then after simultaneous tomography and topography of micro-electro mechanical systems based on silicon ICs. By means of sweeping the frequency of the light source, multiple interferograms were recorded and both amplitude and phase map of the interference fringe signal were reconstructed. Optically sectioned images of the silicon ICs were obtained by selective Fourier filtering and the topography was retrieved from the phase-map. Importance of composite materials has increased tremendously in recent years due to their vast multidisciplinary applications. The full-field SS-OCT was then applied for the structural characterization of composite materials. The present study on the new applications of SS-OCT reveals that OCT has tremendous potential for imaging and detection not only in biological sciences but also in many other areas of science and engineering.

ACKNOWLEDGMENT

The author is thankful to Mr. S. K. Dubey for fruitful discussion and help. The author gratefully acknowledge the financial assistance from Department of Science and Technology, Delhi, Govt. of India for the project No. SR/S2/LOP-02/2003.

REFERENCES

1. D. Huang, E. A. Swanson, C. P. Lin, J. S. Schuman, W. G. Stinson, W. Chang, M. R. Hee, T. Flotte, K.

Gregory, C. A. Puliafito, and J. G. Fujimoto, "Optical coherence tomography," Science **254**, 1178-1181 (1991).
2. B. E. Bouma and G. J. Jearney, *Handbook of Optical Coherence Tomography* (Marcel Dekker, Inc., New York, USA, 2002).
3. M. Brezinski, *Optical Coherence Tomography: Principles and Applications* (Academic Press, Burlington, MA, USA, 2006).
4. P. H. Tomlins and R. K. Wang, "Theory, developments and applications of optical coherence tomography," J. Phys. D: Appl. Phys. **38**, 2519-2535 (2005).
5. R. Leitgeb, C. K. Hitzenberger, and A. F. Fercher, "Performance of Fourier domain vs. time domain optical coherence tomography," Opt. Exp. **11**, 889-894 (2003).
6. J. Kim, C. Choi, and K. S. Soh "Real spectral-domain optical coherence tomography using a superluminescent diode," J. Korean Phys. Soc. **47**, 375-379 (2005).
7. M. A. Choma, M. V. Sarunic, C. Yang, and J. A. Izatt, "Sensitivity advantage of swept-source and Fourier-domain optical coherence tomography," Opt. Exp. **11**, 2183-2189 (2003).
8. S. R. Chinn, E. A. Swanson, and J. G. Fujimoto, "Optical coherence tomography using a frequency-tunable optical source," Opt. Lett. **22**, 340-342 (1997).
9. M. V. Sarunic, M. A Choma, C. Yang, and J. A. Izatt, "Instantaneous complex conjugate resolved spectral and swept-source OCT using 3x3 fiber couplers," Opt. Exp. **13**, 957-967 (2005).
10. H. Lim, J. F. de Boer, B. H. Park, E. C. W. Lee, R. Yelin, and S. H. Yun, "Optical frequency domain imaging with a rapidly sweep laser in the 815-870 nm range," Opt. Exp. **14**, 5937-5944 (2006).
11. M. V. Sarunic, S. Weinberg, and J. A. Izatt, "Full-field swept-source phase microscopy," Opt. Lett. **31**, 1462-1464 (2006).
12. V. J. Srinivasan, R. Huber, I. Gorczynska, and J. G. Fujimoto, "High-speed, high-resolution optical coherence tomography retinal imaging with a frequency-swept laser at 850 nm," Opt. Lett. **32**, 361-363 (2007).
13. P. Blazkiewicz, M. Gourlay, J. R. Tucker, A. D. Rakic, and A. V. Zvyagin, "Signal-to-noise ratio study of full-field Fourier-domain optical coherence tomography," Appl. Opt. **44**, 7722-7729 (2005).
14. B. Považay, A. Unterhuber, B. Hermann, and H. Sattmann, "Full-field time-encoded frequency-domain optical coherence tomography," Opt. Exp. **14**, 7661-7669 (2006).
15. S. K. Dubey, T. Anna, C. Shakher, and D. S. Mehta, "Fingerprint detection using full-field swept-source optical coherence tomography," App. Phys. Lett. **91**, 181106-181108 (2007).
16. S. K. Dubey, D. S. Mehta, A. Anand, and C. Shakher, "Simultaneous topography and tomography of latent fingerprints using full-field swept-source optical coherence tomography," J. Opt. A: Pure Appl. Opt. **10**, 015307-0153015 (2008).
17. T. Anna, C. Shakher, and D. S. Mehta, "Simultaneous tomography and topography of silicon integrated circuits using full-field swept-source optical coherence tomography," J. Opt. A: Pure Appl. Opt. **11**, 045501-045509 (2009).
18. E. Alarousu, L. Krehut, T. Prykari, and R. Myllyla, "Study on the use of optical coherence tomography in measurements of paper properties," Meas. Sci. Technol. **16**, 1131-1138 (2005).
19. H. C. Lee and R. E. Gaensslen, *Advances in Fingerprint Technology*, 2nd ed. (CRC Press, Florida, USA, 2001).
20. G. S. Sodhi and J. Kaur, "Powder method for detecting latent fingerprints: a review," Forensic Science International **120**, 172-176 (2001).
21. F. Hussain, M. Hojjati, M. Okamoto, and R. E. Gorga, "Review article: polymer-matrix nanocomposites, processing, manufacturing, and application: an overview," J. Composite Mat. **40**, 1511-1575 (2006).
22. T. R. Vijayaram, S. Sulaiman, and A. M. S. Hamouda, "Fabrication of fiber reinforced metal matrix composites by squeeze casting technology," J. Mat. Proc. Tech. **178**, 34-38 (2006).
23. A. Dubois, L. Vabre, A. C. Boccara, and E. Beaurepaire, "High-resolution full-field optical coherence tomography with a linnik microscope," Appl. Opt. **41**, 805-812 (2002).
24. G . Moneron, A. C. Boccara, and A. Dubois, "Stroboscopic ultrahigh-resolution full-field optical coherence tomography," Opt. Lett. **30**, 1351-1353 (2005).